AUGMENTED VISION VIDEOPANORAMA SYSTEM FOR REMOTE AIRPORT TOWER OPERATION

N. Fürstenau*, M. Schmidt*, M. Rudolph*, C. Möhlenbrink*, W. Halle**
*German Aerospace Center, Inst. of Flight Guidance, Braunschweig, Germany
**German Aerospace Center, Inst. of Robotics & Mechatronics, Berlin, Germany

Keywords: *Airport Control Tower, Remote Operation, Videopanorama, Augmented Vision*

Abstract

In this paper an experimental high resolution videopanorama system for remote tower operation (RTO) is described and results of initial field test are reported. The reconstructed far view with integrated zoom function serves as main information source for surface movement management of small airports by a remotely located tower controller. It provides the framework for video-see-through augmented vision by integration of traffic data with object tracking and it allows for panorama replay. Evaluation of field tests yields the effective visual resolution of the 180°-video panorama in agreement with the theoretical prediction. A "foveal" component is provided by the remotely controlled pan-tilt zoom camera with a high resolution exceeding the human eye within an observation angle < 15°.

1 Introduction

Remote Tower Operation (RTO) describes the goal of surface movement management of one or more small airports from a remotely located control center without direct far view to the airport surface. Because small airfields usually lack any advanced electronic surveillance system a high resolution augmented vision videopanorama as a potential low cost system is proposed to replace the direct far view out of the tower windows as main component of the Human Machine Interface (HMI) [1][2].

A number of tower work analyses performed during the recent years determined visual surveillance to be the most important activity of tower and apron controllers for creating their situational awareness, despite the availability of electronic surveillance [3][4]. In the tower environment of large airports the permanent refocusing between far view and displays contributes to workload and increases head-down time. Both may be reduced by a high resolution panorama display in a distance to the operator comparable to radar and flight data displays. Consequently it is assumed that under the guideline of human centered automation, the reconstruction of the far view from the control tower of small airports will improve the transition process to a towerless work environment and make it acceptable to the remotely located RTO controller. Within the DLR project RapTOr (Remote Airport Tower Operation Research) an RTO experimental system is realized at the Braunschweig research airport [1][2]. Research was accompanied by a structured work and task analysis [5] and model based simulations of controller's decision processes [6]. A 180° video panorama system was developed as core of the RTO controller's HMI. For designing a compact RTO work environment video see-through augmented tower vision (ATV) was realized by integrating information from real time image processing and electronic surveillance sensors like multilateration into the digital videopanorama. ATV has been proposed by several authors before, however aiming at augmenting the real far view by means of optical see through head mounted displays, e.g.[8]. Recently initial ATV demonstrations with superimposed information in the real tower environment have been performed [1] by using a head-up holographic backprojection display [11] [12].

In section 2 a brief review of the tower work analysis and development of model based simulation are outlined which support the RTO

HMI design. Section 3 describes the augmented vision video panorama system as basis of the experimental RTO system. Results of field trials are described in section 4. Section 5 provides a conclusion and outlook.

2 Work Analysis and Model Based Simulation

The design and development of the new Remote Controller work environment was supported by a cognitive work and task analysis (CWA) [5] by means of structured interviews of domain experts (controllers) from medium sized airports [6]. The formalised results provide the input data for a Formal Airport Control Model (FAirControl) for the simulation of the controller decision making processes at the tower work positions. In [9][10] it is shown how the results of a CWA are transferred into an executable human machine model, based on Colored Petri Nets (CPN) [7] for simulating the controllers work processes in relation to the airport processes. The formal model allows for evaluation of different variants of work organization, supports the design of the new work environment and the monitoring of psychological parameters, e.g. uncovering of reduced situational awareness.

The model is separated into submodels for the human agent (controller), interaction, and the traffic process [2][9][10]. The interaction model defines the controller-process interactions and includes sub networks for description of information resources, such as radio communication and visual perception of the traffic situation. Consequently the human model(s) and machine model(s) can work independently from each other for certain time periods. The state of the airport process model determines the type and content of visual and electronic surface traffic information (e.g. usage of taxiways, landing clearance) which can be acquired and communicated by the controller. The controller model (human model) is implemented as a Formal Cognitive Resource (FCR) Model based on colored Petri nets [10] and serves for the description of controller behaviour in the tower work environment. As most important feature the model considers the motivated character of hu-

man work as related to the limitations of cognitive resources [7].

The executable model supports the identification of controllers' strategies in task organization and pursuance of goals. The formal work process model with graphical representation of the controlled traffic process improves the communication between domain experts and system developers by simulating different traffic situations to establish a basis for a structured interview of those situations. Initial interviews of two senior controllers focused on the visual information from the outside view. They also provided input for the model development. The following list summarizes the most important visual information (rating = 5, from 1 (= not important) to 5), ordered by area / distance:

1. Approach-/ Departure Range (2-3 km, max. 5 km)
- Recognition of A/C, direction of movement

2.All Airfield Areas (Taxi, Apron, Stand)
- Recognition of all active objects (A/C, vehicles, humans, animals)
- Classification of A/C
- Recognize Smoke at A/C

3.Runway Range (800-1500m, max. 2 km)
- Observe Runway state, detect aircraft parts

4.Taxi Area (500-900 m, max. 2 km)
- Recognition and position of passive objects (A/C and parts, vehicles, obstacles)

5.Apron Area (200m)
- Recognize aircraft damage

6.Stand Area
- Recognize Aircraft damage
- Recognition and position of passive objects (luggage, vehicles)

7.RWY / Taxiway Lights
- Monitor Intensity
- Monitor Function

3 Experimental Videopanorama System

3.1 Reconstruction of the Far View

Motivated by the above mentioned relevance of visual information for tower work processes, a high resolution video panorama system was set up at Brauschweig research air-

port as experimental environment for investigation of different aspects of the RTO HMI and development of a demonstrator [1][2][14].

A block diagram of the augmented vision video panorama system is depicted in Figure 1. The sensor component consists of four high resolution (1600 x 1200 pixels) high dynamic range (14 bit/pixel) CCD cameras ($P_{1, 2, 3, 4}$) covering the Braunschweig airport within 180° and a remotely controlled pan-tilt zoom camera (P_5: PTZ).

Fig. 1: Schematic block diagram of augmented vision video panorama system. Wide light arrow indicates visual information for the controller.

The cameras (photo in Fig.1) are positioned ca. 20 m above the airport surface, horizontally aligned on top of a building at the southern boundary of the airport with 100 m distance to Braunschweig tower, 400 m south of the runway 08/26 (1670 m) which extends in E-W direction. The vertical aperture angle of about 20° (half angle with respect to the horizontal line of sight) allows for a closest surveillance distance of about 60 m. For each camera the signals with 25 frames/s are split into two outputs. One feeds the data compression for transmission to the re-

mote RTO HMI, while the other drives the simultaneous real time image processing running on a parallel workstation. Figure 2 shows an aerial view of the Braunschweig research airport indicating camera position and camera viewing sectors.

Fig. 2: Braunschweig research airport with 1.7 km runway 08/26 extending E-W, fiber optic data link (thin yellow lines) connecting sensor containers. Circle with radiating lines indicate panorama camera position and sectors respectively.

A GBit ethernet switch feeds the images from the five sensors into a single mode fiber optic data link which transfers the typically 100 MBit/s data of the panorama system and PTZ over a distance of 450 m to the visualisation system. A second GBit ethernet switch splits the incoming data into five output channels for decompression with one PC per camera. The PCs also synchronize the displays of the four segments. Each camera is remotely controlled with respect to aperture and γ correction. The PTZ camera is controlled with respect to azimuth, vertical angle and zoom (Z = 1 - 23-fold, focal width 3.6 mm – 82.8 mm, corresponding to 54° - 2.5° visual angle).

The Augmented Vision Videopanorama (AVP-) HMI for a single operator / single airport surveillance is shown in Fig. 3. It is based on four high resolution LCD-monitors (UXGA, 1600x1200 Pixels) for displaying the reconstructed panorama and a separate one for display of the remotely controlled PTZ-camera.

Interaction of the operator with the panorama system (cameras, weather station, microphone) is performed via pen touch-input display. For PTZ positioning the target can be defined manually or by automatic movement detection. A rectangular contour is positioned at the respective location of the panorama, defining the target area to be enlarged. With the tracking mode turned on the square moves coherently with the corresponding object. An algorithm for real time movement detection is running on a separate parallel processor of the image compression PCs of each camera.

An overall latency time between image acquisition and panorama visualization of 230 ms – 270 ms was measured by means of a special shuttered laser arrangement. For this purpose a modulated visible laser beam was coupled into the optical fiber downlead to the sender at the camera position. The time difference between the laser light pulses as monitored by one of the cameras viewing the output face of the downlead fiber and a reference pulse from a 3dB fiber coupler at the laser location was measured with a dual trace oscilloscope.

The five recording PC's with the compression software at the camera position allow for storing panorama and zoom data (roughly 40 GByte of data per hour) and provide the possibility of complete panorama replay. This feature was used for the validation experiments (see section 4).

In order to obtain a compact RTO operator HMI which should fit into a typical tower environment of a medium size airport, one of the pen touch-input displays in the console of Fig. 3 is designed to incorporate video panorama control features as well as traffic information, e.g. electronic flight strips. A mini-panorama at the top is updated with 5 Hz and serves for commanding the PTZ camera orientation via pointing of the touch-pen. The display also contains buttons for optical PTZ-parameters and activation of automatic object tracking via movement detection, a virtual joystic as an additional option for PTZ orientation, and weather data.

3.2 Augmented Vision

Within the video panorama real-time aircraft position information is integrated as obtained from the multilateration system at the Braunschweig airport via the aircraft (a/c) transponder. An example is shown in Fig. 4 where in display no.4 (E) a yellow transponder code with multilateration position is shown, indicating a/c position on the approach glide path. Under reduced visibility this Augmented Tower Vision

Fig. 4: Screenshot of camera no. 4 (= E) display showing augmentation during landing. Superimposed glide path (blue), GPS-trajectories (red), multilateration position (yellow, from transponder) and automatic movement detection (violett square).

(ATV) feature allows for localizing the a/c near the correct position because the transponder code, a/c label and numerical information are integrated near the nominal a/c image location in real time. Contours of the movement areas are superimposed on the reconstructed panorama for guiding the operators attention during low visibility to those areas where moving vehicles are expected.

Another example of augmented vision data is the integration of GPS-position information transmitted via ADS-B. An example is shown in Fig. 4 where D-GPS data measured during flight testing are superimposed on the video in the form of flight trajectories (red) which, after geo-referencing are transformed from geographical into display coordinates.

One important advantage of the so called video see-through augmented vision technique using the digital video panorama is the easy integration of augmented vision features. This characteristic avoids the problem of (computational) delay between real scene and augmented information of the optical see-through technology as realized with the head–up and head mounted techniques (e.g. [8]). Initial laboratory experiments and theoretical investigations with superimposed information on the far view addressed the human performance such as response time and head down time reduction by using transparent displays for reducing the number of monitors [11][12], and the problem of spontaneous cognitive switching due to ambiguous stimuli [13].

3.3 Image Processing

Two different strategies were followed for realizing real time image processing, with the initial goal of automatic object tracking with the PTZ camera via movement detection: a) hardware implementation of algorithms on FPGA's, b) software processing with a second processor or core of the multi-processor video-compression PC.

As a first step automatic moving object tracking with the PTZ–camera was realized by method b) with a simple video–frame difference method for object detection. In practice an update rate of 5 Hz was used although theoretically 20 Hz was estimated to be achievable.

3.4 Expected Performance

By using the fundamental relationship $G / B = (g/f - 1) \approx g / f$, with f = focal length = 12.5 mm, g = object distance, G = object size, B = image size, and a CCD pixel size of p = 7.5 μm (+ 0.5 μm gap), the vertical object size at g = 1 km distance corresponding to 1 Pixel is G / B = 0.6 m / 1 Pixel vertical, or ca. 2 arcmin angular resolution, and 1 m / 1 Pixel along the line of sight. The observable resolution at the videopanorama HMI is reduced due to imperfect optics of the camera, the dynamic (illumination dependent) image compression, and resolution of the display system. The optimistic resolution value of about 2' (two times the diffraction limited value of the human eye) may be approached with decreasing camera aperture, which is of course possible only under good light conditions and object − background contrast. For realization of the panorama only 1424x1066 Pixels of each camera (50° viewing angle) are actually used in order to match the 180° panorama angle.

With the known size and distances of static objects on the airfield it is possible to evaluate the practically achieved effective video panorama resolution as compared to the theoretical estimate of 2 arcmin. For verification we used the red-white (1 m squares) multilateration sensor-containers at the end points of the fiber-optic data network as reference objects (see Fig.2, height and width G = 2 m). The nearest containers as captured by the NE and E-looking camera $P_{3,4}$ are located at distances g_E = 400.8 m (Ref.-Obj. 1) and g_{NE} = 588 m (dark blue circle, Ref. Obj. 2) respectively. With the above mentioned lens equation we obtain 7.8 and 5.3 pixels respectively of the camera chip covered by the container images in the vertical direction. Evaluation of single video camera frames (cameras $P3$, $P4$) reveals 8-9 and 5-6 pixels respectively, depending on the selected intensity threshold. The corresponding theoretical vertical display image size is 2.4 mm (ca. 9 Pixels) and 1.6 mm (6 Pixels) respectively. The size actually measured on the displays is 3 mm and 2.5 mm respectively, i.e. 25 and 60 % larger, respectively, than predicted by elementary optics, with a correspondingly reduced value of the angular video resolution α_V as compared to the

theoretical 2 arcmin value: α_V^{exp} = 0.2 m/400.8 m = 1.7 arcmin for Ref.Obj. 1 and α_V^{exp} = 0.24 m/588 m = 1.4 arcmin for Ref.Obj. 2.

The theoretical angular resolution of the PTZ-camera is given by $\alpha_Z = p_H / Z f_0$, yielding the following values (with p_H = horizontal pixel size = 4.4 µm and f_0 (Z = 1) = 3.6 mm.

Zoom Factor Z	α_V arc min	2Θ Degree
3.6	1.09	16.2
4.0	0.98	14.6
23	0.17	2.5

Table 1:Theoretical PTZ resolution and corresponding observation angle for the two Z-factors used in the field tests and for maximum Z = 23.

4 Field Testing and Discussion

The main question to be answered refers to the comparability of the video panorama with the real view out of the tower windows with regard to the control tasks of the operators. For validation of the videopanorama system usability including the zoom function a flight-test plan was set up for experts and non-experts to evaluate identical scenarios under real view and video panorama conditions.

4.1 Experimental Design

Flight tests of two hour duration each, with the DLR DO-228 (D-CODE) test aircraft were designed with successions of approach, touch-and-go (or low approach) and takeoff. Five subjects (2 controllers of the Braunschweig Tower (S_1,S_2) and 3 non-experts (S_3, S_4, S_5, members of the human factors department)) observed the flyby from a position near the panorama camera system and monitored times of 11 characteristic events $e_1 - e_{11}$: out of sight, low / steep dept. angle, takeoff, touchdown, approach main / grass runway, landing gear down / up, steep approach, first sighting. The measurements were performed with notebook (touch input) com-

puters by each subject using a specially designed data input software (GUI). Pilots received the flight plan for up to 16 approaches. One of the GPS trajectories recorded for each flight with the onboard Omnistar satellite navigation system is shown in Fig.5, including event observation positions $x(e_i)$ of the corresponding observation times $t(e_i)$. For the present task of determining the perceived video resolution only the six well defined events with the lowest time variances were used (see Table 2).

The distance between the airport reference point ARP and departure and approach turning points was ca. 4 km and 14 km respectively. Flights were performed under VFR conditions Each flyby was characterized by 6 parameters, with parameter values statistically mixed: 1. approaching main (concrete) or grass runway; 2. approach angle normal or high; 3. landing gear out: early, normal, late; 4. low level crossing of airport or touch and go; 5. touch down point early or late; 6. departure angle normal, low angle, steep angle.

While pilots had a detailed plan to follow for the sequence of approaches with different parameter values, the subjects only knew about the different possibilities (e.g. approach grass or main runway) within the approaches. They had to activate the corresponding field of their input display of the tablet PC and set a time mark at the time of their observation of one out of the 11 possible events during each of the D-CODE approaches / flybys (e.g. a/c visible = first sighting of aircraft, mostly recognized by the head light under the present (weather) conditions). Also all approaches of additional (non-D-CODE) a/c were monitored. Experts and non-experts were briefed separately before the first experiment, with both groups filling separate questionaires.

During test #1 significant time drifts between the individual computers were observed which were corrected for by comparing with the P_1-camera time as reference before and after the 2-hour experiment for generating correction factors. For trials 2, 3 a LAN with time synchronized camera and data acquisition touch-input laptops was used.

On December 13 2006 the first out of three 2-hour trials were performed with lower cloud boundary at 600 m. Two more experiments

were performed in 2007 on May 21 with clear sky and 22 with reduced visibility (< 10 km)
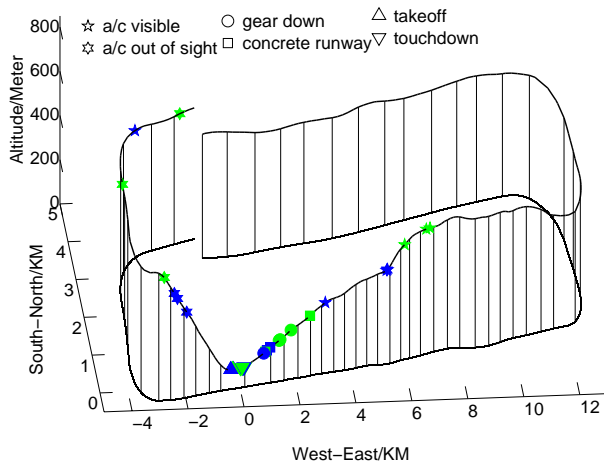
Fig. 5: GPS trajectory no. 4 out of 11 test flights at 13/12/06 (clockwise direction). green / blue symbols represent event observations under real view / video panorama conditions. Approach direction 260° at RWY 08/26 with touchdown near ARP at 0 km (52°19'09" N, 10° 33'22" E). Vertica lines = 10 s intervals on flight trajectory. Final speed ca. 100 kn.

4.2 Experimental Results: Videopanorama

For each trial raw data from all subjects and for all approaches under real view conditions were collected into a single data file. Evaluation of the different approach, touch-and-go, and departure conditions (in trial #1 14 approaches with 11 D-CODE and 3 other aircraft) yields the inter-subject time measurement scattering with mean and standard deviation (stdev) of the sample and standard errors (sterr) of mean for the n = 5 subjects.

In trial #1 typical unbiased estimates of sample stdev for event e_{11} (first sighting during approach) were between 2 s and 25 s (sterr = 1 – 15 s). Comparing approach recognition time with low stdev with the GPS track yielded first sighting of a/c (headlight) at distance 9 km. The minimum sterr. of e.g. 1 s for e_{11} and 0.2 s for e_5 (touchdown) presumably represent the optimum observation conditions for all subjects (i.e. all n = 5 attending first sighting direction during expected apearance time).

Detailed information on the difference between real view and video panorama are obtained by repeating the experiments with the video panorama replay after a week or more in order for the subjects to no longer remember the different flight conditions. It was expected that due to lower resolution of the videopanorama (theoretical estimate $\alpha_V \approx 2$ arc min, see section 3) as compared to the real view, distant events of approaching / departing a/c (like first / last sighting of a/c) should receive an earlier/later mark under real view as compared to video observation. Correspondingly within-subject evaluations of the direct viewing and video panorama replay observations yields time differences $t(\text{real view}, e_i) - t(\text{video}, e_i) < 0$ and > 0 for approaching (app) and departing (dpt) a/c respectively.

Results of the initial trial #1 were reported in [2][14], showing experimental visual resolution between 1.3 and 2 arcmin in reasonable agreement with the theoretical prediction and with the verification measurements. In Table 2 the results for six of the 11 possible observation types are shown for the trials #2, 3 (May 21, sunny day & 22/07, cloudy day), for all subjects and all those flights with pairs of observation (time marks) of real view − video, with no. of observation pairs N, mean Δt(real view - video), standard deviation and std. error of mean.

All displayed events exhibit reproducible and significant pos.(dpt.) and neg.(app.) delays between video panorama and real view conditions. For example the significant negative delay measured as overall mean for e_8 (landing gear visible, -13.0 ± 2.0 s and -13.2± 1.2 s respectively) shows this event to be observable with video only 0.7 km closer to the airport (a/c speed ca. 100 kn = 185 km/h), as compared to the real view conditions (e.g. e_{11}(real view): a/c (lights) recognized at ca. 8 km). If we assume that detection time difference is determined by the difference of optical resolution between real view (resolution of the human eye ca. $\alpha_E \approx 1$ arcmin = 1/60 °) and videopanorama system, the measured time difference Δt(real view-video) = $t_E − t_V$ from table 2 can be used for calculating the effective resolution α_V of the optical system.

Trial #2 (clear) Event e_i	N	Mean Δt / s	S.D. / s	S.E. / s
e_{11}: A/C visible	54	-85.1	77.9	10.7
e_8: Gear visible	42	-13.0	12.9	2.0
e_6: main RWY	28	-34.3	49.5	9.5
e_7: grass RWY	22	-29.4	45.5	9.9
e_5: touchdown	22	+1.8	1.0	0.2
e_4: takeoff	17	+2.3	2.5	0.6
Trial #3(cloudy) Event e_i	N	Mean Δt / s	S.D. / s	S.E. / s
e_{11}: A/C visible	54	-26.5	18.3	2.5
e_8: Gear visible	44	-13.2	7.6	1.2
e_6: main RWY	28	-15.7	16.0	3.1
e_7: grass RWY	20	-25.8	24.5	5.6
e_5: touchdown	25	+2.0	1.0	0.2
e_4: takeoff	23	+2.0	1.4	0.3

Table 2: Trial #2(May 21/07, clear view, > 10 km) and #3(May22/07, cloudy, < 10 km). Mean, standard deviation and std. error of event observation time difference Δt = t(real view)–t(replay).

For suitable events with known object size the single Δt-values allow for calculation of α_V via:

$$\alpha_V = \alpha_E \left(1 + \alpha_E v_E \Delta t/G \right)^{-1} \qquad (1)$$

where the resolution angle α is given by $\alpha_{E,V}$ = G / $x_{E,V}$ measured in rad, with event observation distance $x_{E,V}$ under real view (E) and video replay (V) conditions. G is the object size, e.g. aircraft cross section for e_{11} or landing gear wheel size for e_8. For e_8 we obtain in this way $\alpha_V = 1.4 \, \alpha_E$ (with G(main wheel) = 0.65 m, v_E = 100 kn). For e_{11} (using G(cabin) = 1.8 m) trial #3 yields 1.3 α_E. Both values are in agreement within the experimental uncertainty, although smaller (even better) than the theoretical estimate.

The extremely large observation time difference and s.d. of e_{11} in trial #2 is due to real view event registration under clear view conditions (mostly expert subjects S1, S2) long before the a/c turned towards approach at the ILS turning point. In order to obtain a statistically relevant and model based mean value, a linear regression procedure is employed for those events where the optical resolution (more or less modified by image contrast) may be assumed to play the dominant role for event timing. Because e_1 was unreliable due to observability problems (the aircraft quite often vanished from the P1-camera observation angle before e_1 was observable), only e_4, e_5, e_8, e_{11} were used for this evaluation. For applying a regression procedure the independent variable "event e_i" has to be replaced by a quantifiable variable. A linear model is obtained when considering the observation distance x as obtained from the GPS reference trajectory instead of the observation time, yielding the $\Delta x(E - V) = v_E(t) \Delta t$ versus x_E dependence for regression analysis as depicted in Fig. 6 for trial #3 (cloudy day).
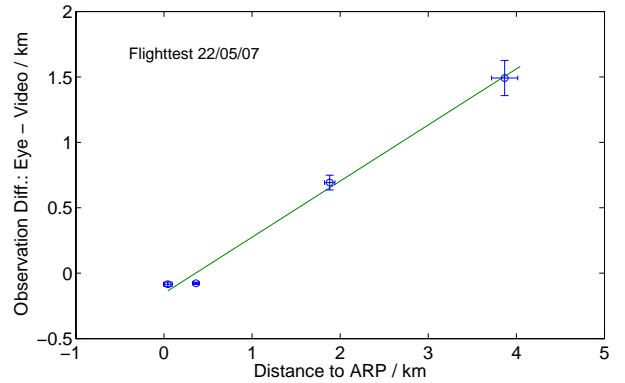
Fig. 6: Mean event-observation position differences Δx (real view – video replay) between real far view and video panorama conditions versus mean GPS-position estimate of x_E (= distance from event position x_E to airport reference point ARP) for trial #3. Error bars represent S.E. of means. Straight line: linear regression.

The scatter plot of the four data points (x_E, $\Delta x = v_E\Delta t$, for e_4, e_5, e_8, e_{11}) is obtained by correlating the measured time values with the corresponding GPS position data. For data fitting the theoretical relationship

$$\Delta x\left(eye - video\right) = \left(1 - \alpha_E/\alpha_V\right)x_E \qquad (2)$$

$$\alpha_V = \alpha_E \left(1 - \beta_1\right)^{-1} \qquad (3)$$

is employed. With the slope $\beta_1 = \Delta x/x_E = 0.429$ (± 0.02 std.err., $R^2 = 0.99$, significance level $F = 321$ at $p = 0.003$) the corresponding α_V estimate of 1.75 arcmin (± 0.08) is obtained, exhibiting even better agreement with the predictions of section 3.4 than the initial trial #1, reported in [14].

4.3 Experimental Results: Zoom Function

In order to decrease the duration of the replay experiments for evaluating observations with the PTZ camera (e11, e8) only the approach sections of the videos until touchdown (event e_5) were used. Because due to this procedure time synchronization with real-view experiments was lost, PTZ experiments were related to panorama replay with touchdown time as common reference. For data evaluation equation (1) with substitution of a_V through α_{PTZ} and α_E through a_V was used, yielding

$$\alpha_{PTZ} = \alpha_V \left(1 + \alpha_V v\Delta t/G\right)^{-1} \qquad (4)$$

The experimental results for the effective PTZ resolution are presented in table 3.

Trial #2 & 3	α_{PTZ} / arcmin for (Δt / s)	
Zoom Factor Z (2Θ)	e11: 1st Sighting	e8: Gear down
3.6 (16.2°)	1.07 (52)	1.35 (10)
4.0 (14.5°)	1.30 (32)	1.23 (14)
Mean	1.2 (42)	1.3 (12)

Table 3: PT-Zoom experiment for determining effective resolution. Δt = measured event observation time difference t(Panorama) – t(PTZ). Z = 3.6: day 1, clear; Z = 4: day 2: cloudy.

They are reasonably close to the theoretical value $\alpha_{PTZ} \approx 1' = \alpha_E$ as obtained under the hypothesis of resolution based object detection times (see Table 1). These data were obtained with 20 subjects observing those three rounds around the airport each of the two days, which included a touchdown (e_5) to be used as com-

mon PTZ – videopanorama reference with Δt (Panorama – PTZ) ≈ 0 s.

4.4 Image Processing: Movement Detection

The basic performance of the software based movement detection algorithms (strategy b) of section 3.3) is observable with automatic PTZ-tracking activated. It demonstrates the practical usefulness of this feature, however with limited reliability due to relatively simple algorithms based on image subtraction and texture analysis of detected clusters.

For increasing reliability algorithms have to be matched to the basically different features below horizon (e.g. use of masks for disregarding non-movement areas, masking trees and bushes with texture analysis) and above horizon (discriminate moving aircraft from moving clouds). An example is shown in Fig. 7.
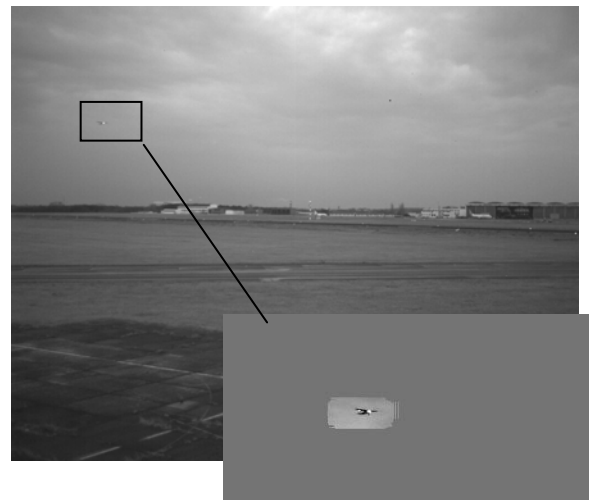
Fig. 7: Detection of small aircraft among moving clouds with automatic background subtraction

Using offline processing with algorithms developed under IDL within strategy a), aircraft are detected in the sky with moving clouds. Background is automatically subtracted. Detection relies on combination of different criteria: 1. speed (a/c faster than clouds), 2. a/c texture different from clouds.

5 Summary and Conclusion

Basic elements of DLR's experimental Remote Tower Operation (RTO) system at the Braunschweig Research Airport are described which is being developed under the guideline of human centered automation. Initial field test results are reported which are evaluated by assuming the optical resolution to play the dominant role for event detection. Quantitative evaluation of field trials for comparing real view and video panorama observation verifies the theoretically predicted video panorama and PTZ resolution of ca. 2 arcmin and ca. 1 arcmin (with Z=4) respectively. The latter one corresponds to the foveal resolution of the human eye and exceeds it with increasing Z, approaching the physical diffraction limit. One planned extension of the augmented vision videopanorama system is the inclusion of cost effective sensors covering additional spectral ranges (IR, mm-wave). Another is the extension of the augmented vision function into an active visual assistance system by enhanced usage of automatic image processing as part of the ASMGCS data fusion system including the autonomous control option of the PTZ-camera. A follow-up project will also address more realistic shadow mode testing.

References

[1] Schmidt, M., Rudolph, M., Werther, B., Fürstenau, N.: Remote Airport Tower Operation with Augmented Vision Video Panorama HMI. *Proc. 2nd Int Conf. Res. in Air Transportation ICRAT*, Belgrade (2006) 221 – 230

[2] Schmidt, M., Rudolph, M., Werther, B., Möhlenbrink, C. Fürstenau, N.: Development of an Augmented Vision Video Panorama Human-Machine Interface for Remote Airport Tower Operation. In: *M.J. Smith, G. Salvendy (Eds.) Human Interface II, Lect. Notes Computer Science 4558*, pp. 1119-1128, Springer-Verlag Berlin Heidelberg (2007)

[3] Tavanti, M.: Control Tower Operations: A Literature Review of Task Analysis Studies. *EEC Note 05* (2006)

[4] Pinska, E.: An Investigation of the Head-up Time at Tower and Ground Control Positions. *Proc. 5th Eurocontrol Innovative Research Workshop* (2006) 81-86

[5] K.J. Vicente, *Cognitive Work Analysis,* Mahwah/NJ: Lawrence Erlbaum Associates, 1999.

[6] Werther, B., Uhlmann, H.: Ansatz zur modellbasierten Entwicklung eines Lotsenarbeitsplatzes. In: *Zustandserkennung und Systemgestaltung,* Fortschritt Berichte VDI, 22 (2005) 291 -294.

[7] Werther, B.: Kognitive Modellierung mit farbigen Petrinetzen zur Analyse menschlichen Verhaltens. *PhD Dissertation,* DLR-Inst. of Flight Guidance, (2006).

[8] Ellis, S.: Towards determination of visual requirements for augmented reality displays and virtual environments for the airport tower. *Proc. NATO workshop on Virtual Media for the Military,* West Point /N.Y., HFM-121/RTG 042 HFM-136, (2006) 31-1-31-9

[9] Werther, B.: Colored Petri net based modeling of airport control processes. In: *Proc. Int. Conf. Comput. Intelligence for Modelling, Control & Automation (CIMCA)* Sydney (2006) IEEE ISBN 0-7695-2731-0

[10] Werther, B., Schnieder, E.: Formal Cognitive Resource Model: Modeling of human behavior in complex work environments, in: *Proc. Int. Conf. Computational Intelligence for Modelling, Control & Automation (CIMCA 2005),* Wien: 2005, pp. 606 – 611.

[11] N. Fürstenau, M. Rudolph, M. Schmidt, B. Lorenz, T. Albrecht, "On the use of transparent rear projection screens to reduce head – down time in the air – traffic control tower", in: *Proc. Human Performance, Situation Awareness and Automation Technology (HAPSA II),* Mahwah/NJ: Lawrence Erlbaum Publishers Inc., 2004, pp. 195 – 200

[12] Peterson, S., Pinska, E.: Human Performance with simulated Collimation in Transparent Projection Screens. *Proc. 2nd Int. Conf. Res. in Air Transportation,* Belgrade (2006) 231-237.

[13] Fürstenau, N.: Modelling and Simulation of spontaneous perception switching with ambiguous visual stimuli in augmented vision systems. *Lecture Notes in Artificial Intelligence 4021 (2006)* Springer-Verlag, Berlin, New York, 20-31

[14] N. Fürstenau, M. Schmidt, M. Rudolph, C. Möhlenbrink, B. Werther. Development of an Augmented Vision Videopanorama Human-Machine Interface for Remote Airport Tower Operation, in: *Proc. 6th Eurocontrol Innovative Res. Workshop,* Eurocontrol Experimental Center, Bretigny (2007) 125-132

Copyright Statement